Succinylation of H3K122 destabilizes nucleosomes and enhances transcription

Lara Zorro Shahidian[1], Mariska Haas[2], Stephanie Le Gras[3,4], Sandra Nitsch[1], André Mourão[5], Arie Geerlof[5], Raphael Margueron[6], Jens Michaelis[2], Sylvain Daujat[3,†] & Robert Schneider[1,7,8,*]

Abstract

Histone post-translational modifications (PTMs) are key players in chromatin regulation. The identification of novel histone acylations raises important questions regarding their role in transcription. In this study, we characterize the role of an acylation on the lateral surface of the histone octamer, H3K122 succinylation (H3K122-succ), in chromatin function and transcription. Using chromatin succinylated at H3K122 in *in vitro* transcription assays, we show that the presence of H3K122succ is sufficient to stimulate transcription. In line with this, we found in our ChIP assays H3K122succ enriched on promoters of active genes and H3K122succ enrichment scaling with gene expression levels. Furthermore, we show that the co-activators p300/CBP can succinylate H3K122 and identify sirtuin 5 (SIRT5) as a new desuccinylase. By applying single molecule FRET assays, we demonstrate a direct effect of H3K122-succ on nucleosome stability, indicating an important role for histone succinylation in modulating chromatin dynamics. Together, these data provide the first insights into the mechanisms underlying transcriptional regulation by H3K122succ.

Introduction

The organization of DNA into chromatin allows the DNA to be stored within the nucleus of a cell, while at the same time safe-guarding, when necessary, its accessibility. Histones are the main protein component of chromatin (Luger *et al*, 1997). Multiple studies have described how different post-translational modifications (PTMs) on the histone N-terminal tails, which extend from the nucleosomal core, indirectly regulate chromatin function, e.g., by recruiting or excluding binding proteins (Jenuwein & Allis, 2001). However, more direct effects of histone PTMs are still poorly understood (Kouzarides, 2007; Lawrence *et al*, 2016).

Histone post-translational modifications can occur, apart from the N-terminal tails, also within the globular domains of histones (Mersfelder & Parthun, 2006; Tropberger & Schneider, 2013). In addition to acetylation, multiple different histone acylations have been identified within the nucleosomal core, including butyrylation, crotonylation, malonylation, and succinylation (Tan *et al*, 2011; Tessarz & Kouzarides, 2014; Kebede *et al*, 2015). All these modifications change the charge of the side chain of the modified lysine residue and thus can, depending on their position, potentially alter the interactions with other histones, neighboring nucleosomes or with the nucleosomal DNA (Mersfelder & Parthun, 2006).

Several studies have shown that lysine acetylations within the globular domain of histones can affect nucleosome stability (Neumann *et al*, 2009; Tropberger *et al*, 2013; Di Cerbo *et al*, 2014) and regulate chromatin-dependent processes (Lawrence *et al*, 2016). Namely, the acetylation of histone H3K122 (H3K122ac), located on the so-called lateral surface of the histone octamer, can directly increase transcriptional output (Tropberger *et al*, 2013). Recently, Bao *et al* (2019) described that a new type of acylation, glutarylation of lysine 91 on histone H4 (H4K91glut), impairs the interaction between the H3-H4 tetramer and the H2A-H2B dimers, resulting in the destabilization of the nucleosome.

Lysine succinylation was first described in Zhang *et al* (2011), and a year later, the succinylation of H3K122 (H3K122succ) was identified by mass spectrometry (Xie *et al*, 2012). It converts, in contrast to the majority of other acylations, the positive charge of the lysine residue to a negative charge and increases the steric hindrance due to its larger volume. Lysine succinylation could therefore affect interactions involving the lysine side chain. Interestingly, H3K122 is positioned on the dyad axis of the nucleosome,

1 Institute of Functional Epigenetics, Helmholtz Zentrum München, Neuherberg, Germany
2 Institute of Biophysics, Ulm University, Ulm, Germany
3 IGBMC, CNRS UMR7104, Inserm U1258, Université de Strasbourg, Illkirch, France
4 Plateforme GenomEast, Infrastructure France Génomique, Cedex, France
5 Protein Expression and Purification Facility, Helmholtz Zentrum München, Neuherberg, Germany
6 Institut Curie, INSERM U934, CNRS UMR3215, Paris, France
7 German Center for Diabetes Research (DZD), Neuherberg, Germany
8 Faculty of Biology, Ludwig-Maximilians Universität München, Planegg-Martinsried, Germany
*Corresponding author. Tel: +49 89 31870; E-mail: robert.schneider@helmholtz-muenchen.de
†Present address: Biotechnology and Cell Signaling, CNRS UMR7242, University of Strasbourg, Cedex, France

where its side chain is in contact with the nucleosomal DNA. Any perturbation of the dyad axis conformation has the potential to affect nucleosome dynamics, as this is the region where the nucleosomal DNA and the histone octamer are in closest proximity and their interactions are the strongest (Cutter & Hayes, 2016). Previously, the desuccinylation of H3K122succ by sirtuin 7 (SIRT7) has been shown to be associated with DNA double strand break repair and genome stability (Li *et al*, 2016); however, the role of H3K122-succ in transcription is still unclear.

The important location of H3K122 and the reversal of the charge of lysine 122 by succinylation prompted us to study the possible role of H3K122 succinylation in transcription. Here, we find by using our new antibodies H3K122succ enriched on the promoter regions of actively transcribed genes and we identify novel enzymes responsible for the establishment and removal of this mark. By comparing site-specific succinylated chromatin with unmodified chromatin, we demonstrate that H3K122succ is sufficient to increase transcriptional output. We reveal that H3K122succ destabilizes nucleosomes and, thus, gain insights into potential mechanisms on how H3K122succ acts.

Results and Discussion

In order to specifically study H3K122succ, we raised and affinity purified three rabbit polyclonal antibodies (ABs) against H3K122-succ. All three ABs recognized in peptide dot blot assays the immunizing H3K122succ peptide with no cross-reactivity observed to any other peptide tested (Figs 1A and EV1A and B). In immunoblot, all ABs recognized H3 specifically and this signal was competed away by the H3K122succ peptide (see Fig EV1C for an example). Succinylated H3, but not equal amounts of unmodified H3 nor H3 mutated on K122 to an arginine (Fig 1B) were detected. Additionally, also in native chromatin (ChIP input) H3 was specifically recognized (Fig EV1D) and this reactivity did not depend on the presence of the H3 N-terminal tail (Fig EV1E). Taken together, these data demonstrate the specificity of our ABs for H3K122succ in native chromatin as well as on histone peptides.

H3K122succ is enriched at transcription start sites

We next investigated the genomic distribution of this modification by carrying out native chromatin immunoprecipitation followed by deep sequencing (ChIP-seq) on the human MCF7 breast cancer cell line using all three independent antibodies against H3K122succ. We identified in our ChIP 4745, 4788, and 4346 peaks with AB #1, AB #2, and AB #3, respectively. Reads enrichment in all H3K122succ

peaks were highly correlated (Spearman's $\rho \geq 0.9$, Fig 1C). We found that H3K122succ peaks obtained in our ChIP experiments with all three antibodies were preferentially located in gene promoter regions ($\geq 50\%$) and specifically close to and at transcription starting sites (TSS), with 46–49% of H3K122succ peaks at TSS regions, compared to only 5% in a random peak set (Fig 1D). This localization of H3K122succ peaks to TSS regions suggests that H3K122succ may play a role in transcriptional regulation.

H3K122succ marks active genes

Since our three antibodies gave consistent results, we focused on AB #2 for all subsequent analysis. A first visual inspection of the genome browser tracks revealed an enrichment of H3K122succ around the TSS of active genes together with other histone modifications (Fig 2A). Approximately three-quarters (76.6%) of the genes with H3K122succ ChIP-seq peaks detected at their TSS have CpG island (CGI) containing promoters and more than one-third (35.2%) are housekeeping genes (HKGs; Fig 2B). Furthermore, genome wide our H3K122succ ChIP peaks co-localized with peaks for two hallmarks of active promoters (Santos-Rosa *et al*, 2002)—H3K4me3 and H3K9ac (Fig 2C). More specifically, at TSS 70–80% of the H3K122-succ peaks we detected were also marked with "active" histone tail modifications such as H3K4me3, H3K9ac, and H3K27ac (Fig 2D). When comparing enrichment profiles at the positions of our H3K122succ ChIP peaks with datasets for the histone acetyltransferase p300 and the acetylated histone variant H2A.Z, previously shown to occur on active regulatory regions (Giaimo *et al*, 2019), we found enrichment of p300 and H2A.Zac at the majority of H3K122succ peaks (Fig EV2A). Additionally, the H3K122succ peaks overlapped with open chromatin regions identified both by FAIRE-seq and DNase-seq, at TSS (Fig 2E) and overall (Fig EV2B). Taken together, this suggests that H3K122succ marks promoters of genes in an open and "active" chromatin environment. Indeed, comparison with RNA-seq data revealed that the H3K122succ ChIP-seq read density at TSS correlated with the mRNA levels (Fig 2F). Thus, local H3K122succ enrichment can be indicative of the steady-state mRNA level of the respective gene.

We next examined the relationship between gene expression level and the presence of H3K122succ alone and/or in combination with H3 tail modifications (K4me3, H9ac, and K27ac; Fig 2G). In general, we found that genes with H3K122succ peaks at their TSS (peaks $\pm$ 500 bp around TSS) were more expressed than genes without H3K122succ peaks. Genes where we detect H3K122succ in combination with the three other active marks (H3K9ac, H3K27ac, and H3K4me3) showed the highest expression level of all the groups tested, higher than ones without H3K122succ peaks. To investigate

---

Figure 1. H3K122succ peaks localize to gene promoters.

A Peptide dot blot array probed with anti-H3K122succ AB #2. Peptides with indicated modifications were spotted on membranes. Peptide sequences can be found in Table 1. For other two antibodies, see Fig EV1A and B.

B Immunoblot analysis with anti-H3K122succ AB #2 on indicated histone octamers. Octamers with H3K122succ are specifically recognized.

C Pairwise scatterplots of H3K122succ read counts within peaks from ChIP experiments using all three H3K122succ antibodies (AB #1, AB #2, and AB #3). Note high degree of correlation as indicated by the Spearman correlation coefficient ($\rho \geq 0.9$).

D Genomic feature distribution of H3K122succ peaks obtained with the three H3K122succ antibodies. The percentage of peaks in the 1st exon, remaining exons, intergenic regions, 1st intron, other introns, promoter/ TSS (≤ 1 kb from TSS), promoter (1–2 kb), and 3′ UTR is displayed. A random distribution of peaks is shown for comparison (see Materials and Methods for additional information on the random distribution).
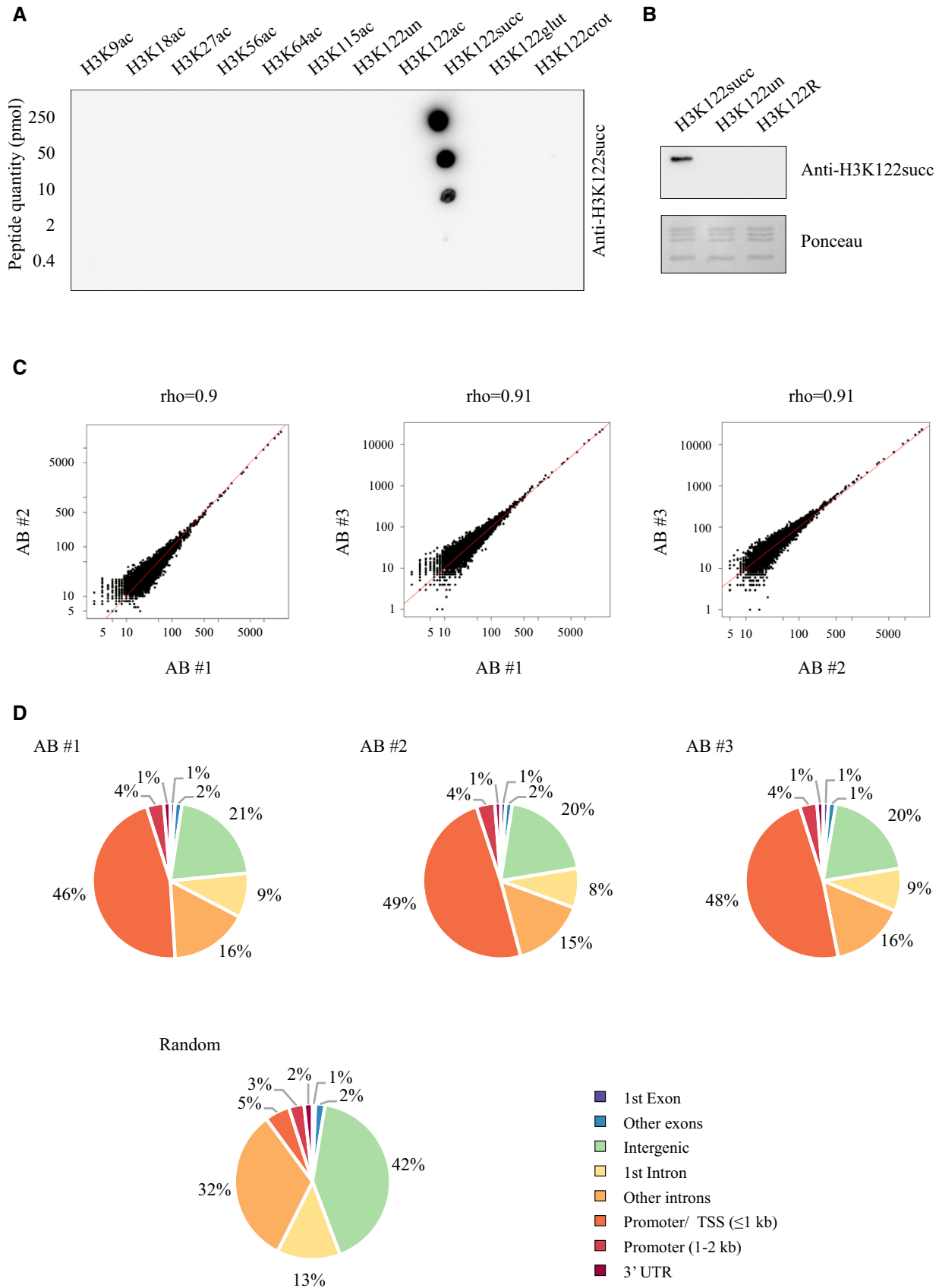
Figure 1.

whether the higher transcription levels simply reflected higher acetylation levels on the histone tails, we used H3K27ac as an example and compared the number of H3K27ac read in these different gene groups (Fig EV2C). These results show that the gene group associated with the highest transcription levels (H3K122succ + 3 histone tails) did not have the most H3K27ac reads, indicating that the higher expression of genes enriched in H3K122succ cannot simply be explained by, e.g., higher H3K27 acetylation levels.

H3K122 can not only be succinylated but also acetylated (Tropberger et al, 2013). We therefore compared the genes we associated with H3K122succ at their TSS with the ones with H3K122ac peaks (Fig EV2D) and found an overlap of 61%. Overall, the number of H3K122succ peaks we detected was lower than the ones for H3K122ac what is in line with the lower overall abundance of histone succinylation compared to histone acetylation (Xie et al, 2012) and could suggest a more specific function for histone succinylation compared to acetylation. However, we cannot rule out that different antibodies affinities or linear ranges of antibodies contribute to the differences in the peak numbers. Interestingly, we found that genes at which we detect H3K122succ peaks at their TSS were in general higher expressed than those with H3K122ac peaks (Fig EV2E). Further studies will be needed to determine whether and how these marks are functionally connected.

Taken together, these results suggest that H3K122succ may promote transcriptional activation and could play a role in creating an optimal chromatin environment allowing for maximal transcriptional output together with other histone modifications.

p300/ CBP can establish H3K122succ

To address the role of H3K122succ in transcriptional regulation, we first sought to identify the enzyme(s) catalyzing the succinylation of H3K122. It has been shown that histone acetyltransferases (HAT) can succinylate proteins (Hirschey & Zhao, 2015; Wang et al, 2017). Therefore, we depleted selected HATs by small interfering RNA (siRNA; Fig EV3A) and assayed the levels of H3K122succ by immunoblot (Figs 3A and EV3B). As shown in Fig 3A, upon double knock down (KD) of p300 and its paralogue CREB binding protein (CBP), we observed decreased levels of H3K122succ. Additionally,

we treated MCF7 cells with curcumin, a p300/ CBP inhibitor (Morimoto et al, 2008) that promotes degradation of p300 and CBP. Indeed, upon curcumin treatment we detected decreased levels of H3K122succ (Fig EV3C). To demonstrate that p300 can catalyze H3K122succ in vitro, we performed next succinyltransferase assays with recombinant p300 on recombinant histone octamers (rOctamers; Figs 3B and EV3D), as well as on peptides spanning the region around H3K122 (Fig 3C) as substrates. In these assays, recombinant p300 can indeed succinylate H3 at position K122. Next, we compared how adding unlabeled acetyl-coa (ac-CoA) or succinyl-CoA (suc-CoA) affects radioactive in vitro histone acylation assays (Fig EV3E). Although suc-CoA can compete, ac-CoA has a stronger effect on signal intensity. Thus, we suggest that the local availability of CoAs, e.g., in metabolic microniches (Katada et al, 2012), could determine if p300 acts as acetyl or succinyltransferase.

In summary based on our in vitro and in vivo assays, we conclude that p300 can succinylate a specific histone residue. This is in line with previous findings that p300 can act as a lysine succinyltransferase in vitro (Hu et al, 2014), as well as with the co-localization between H3K122succ and p300 enrichment that we observed (Fig EV2A). Whether (and which) other enzymes contribute to H3K122 succinylation and whether p300 can succinylate additional residues in histones is still an open question.

Sirtuin 5 can desuccinylate H3K122

Sirtuins have been identified as protein desuccinylases (Maurer et al, 2012). Specifically sirtuin 5 (SIRT5) has been reported as a protein desuccinylase (Du et al, 2011) and, more recently, SIRT7 as an enzyme that can desuccinylate H3K122succ during DNA damage response (Li et al, 2016). Although SIRT5 is mainly a mitochondrial enzyme, it can also be found in the cytosol and in the nucleus (Hirschey & Zhao, 2015).

To explore the role of SIRT5 in the removal of H3K122succ, we performed in vitro desuccinylase assays on H3K122succ peptides with recombinant SIRT5 and SIRT7 (Figs 3D and E, and EV3F and G). As expected, SIRT7 can desuccinylate H3K122; however, SIRT5 can also desuccinylate H3K122. To confirm the activity of SIRT5 in vivo, we compared the levels of H3K122succ on histones isolated

---

Figure 2. H3K122succ is enriched at active TSS.

A IGV browser snapshots showing the distribution of reads around the TSS of the actively transcribed PPM1D gene (chr17:60,587,313-60,643,064; top panel) and of the inactive CD40 gene (chr20:46,114,180-46,129,721; bottom panel) for the indicated histone modifications, input, and RNA-seq.

B Venn diagrams showing the overlap between genes with H3K122succ peaks detected at their TSS regions and genes with CpC island associated to their promoters (CGI) (upper panel), as well as housekeeping genes (HKG) (bottom panel). P-values were calculated through hypergeometric tests.

C Venn diagram showing the number of H3K122succ peaks detected overlapping with H3K4me3 peaks and H3K9ac peaks.

D Correlation matrix displaying the degree of overlap between H3K122succ, H3K4me3, H3K9ac, and H3K27ac peaks from our ChIP experiments at TSS (peaks within ± 500 bp of TSS). Total number and fraction of overlapping peaks are displayed.

E Correlation matrix displaying the overlap between our H3K122succ ChIP-seq peaks and DNase-seq and FAIRE-seq enriched regions at TSS (peaks within ± 500 bp of TSS). Total number and percentage of overlapping peak regions are displayed.

F H3K122succ occupancy profile over a meta gene as a function of expression level (based on RNA-seq quartiles: Q1—least expressed, Q4—most expressed). All genes were normalized to the same length.

G Boxplots visualizing expression values of genes (reads per kb; RPK) with peaks for indicated different combinations of histone PTMs at their TSS. Histone modifications are (from left to right): none (no PTM, black); only H3K122succ (green); H3K122succ plus one tail modification (H3K4me3, or H3K9ac, or H3K27ac, green and light orange); H3K122succ plus two tail modifications (green, yellow, and light orange); H3K4me3 and H3K9ac and H3K27ac without H3K122succ (yellow, light orange, and dark orange); H3K122succ and all three tail modifications (green, yellow, light orange, and dark orange). The number of genes within the groups is indicated below each boxplot. Boxes indicate the range between the first and third quartile, the central line depicts the median, and the whiskers span the range of the data while extending no further than 1.5 times the interquartile range. Each distribution was compared to the "no PTM" distribution. P-values were calculated by Wilcoxon signed-rank test.
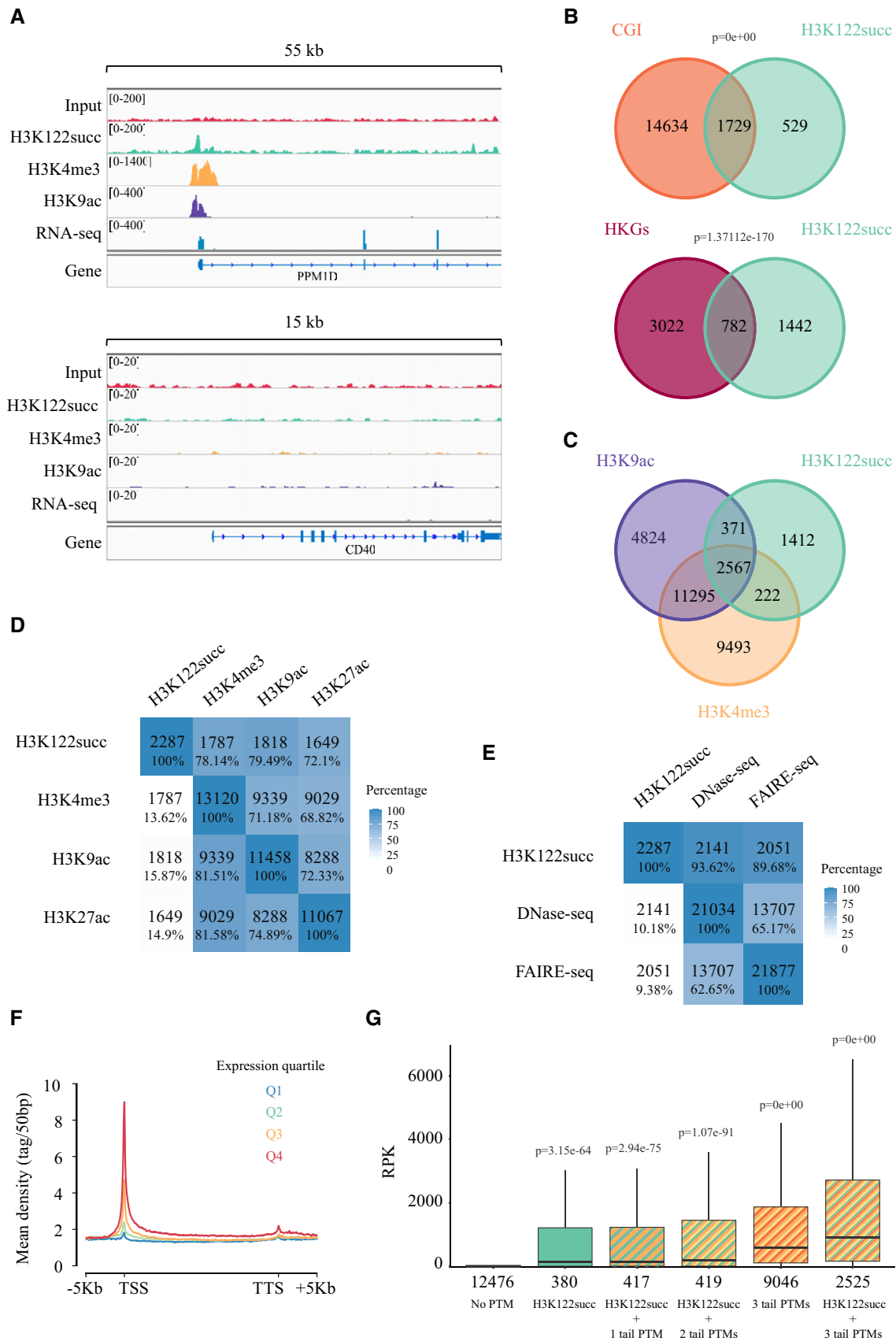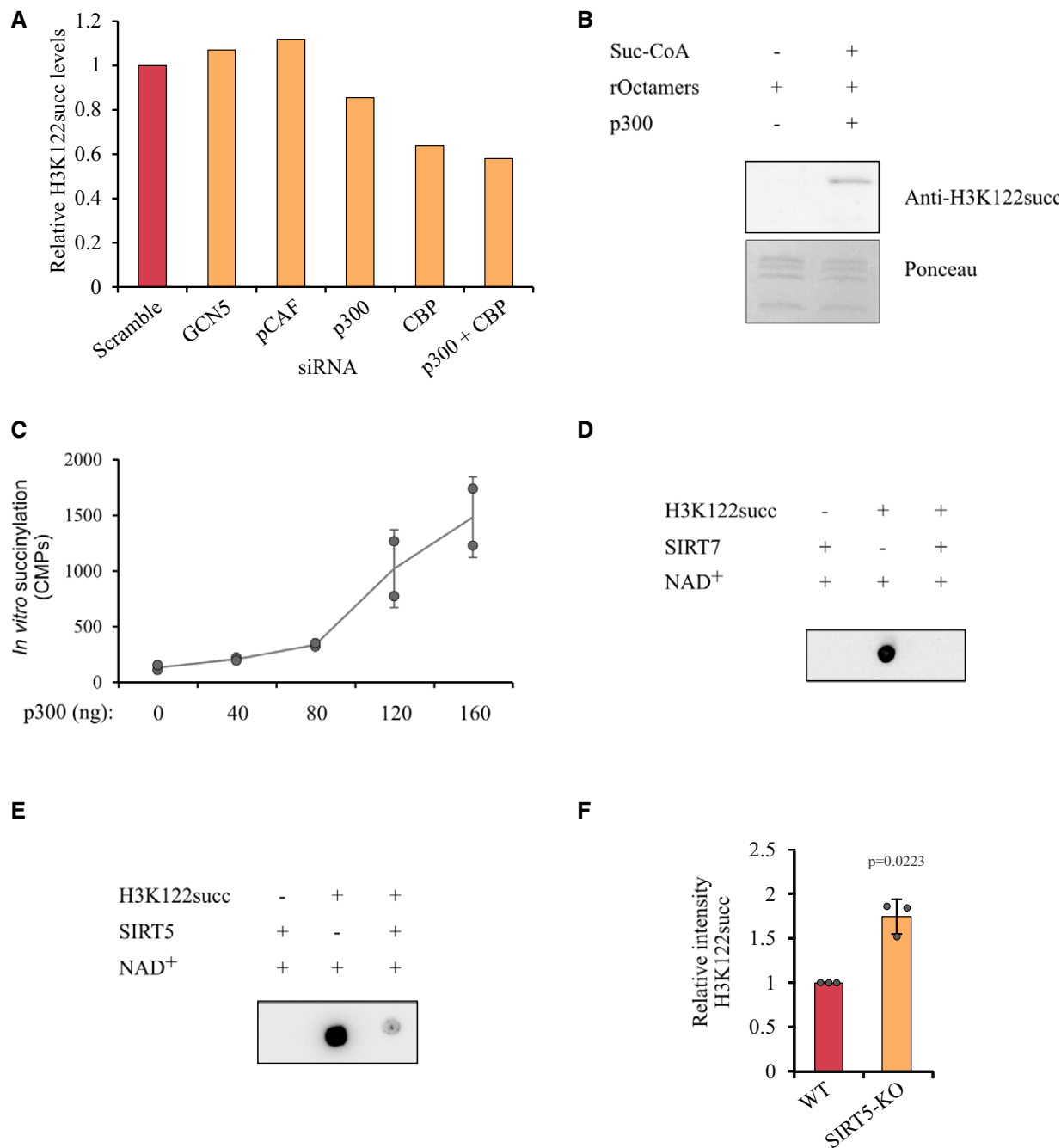
Figure 2.

Figure 3. p300/ CBP can succinylate H3K122, SIRT5 and SIRT7 desuccinylate it.

A   H3K122succ levels (detected by immunoblot), relative to the scramble siRNA control, upon depletion of indicated HAT enzyme(s) (GCN5, pCAF, p300, and/or CBP) from MCF7 cells by siRNA. The bar graph shows a representative experiment (for biological replicate see Fig EV3B).

B   *In vitro* succinyltransferase assay on recombinant histone octamers as substrate. After incubation with p300 and suc-CoA, the H3K122succ levels were assessed by immunoblot. Ponceau staining of membrane is shown as a loading control. For additional controls, see Fig EV3D.

C   *In vitro* succinyltransferase assay on unmodified peptides spanning H3K122. Samples were incubated with increasing amounts of p300 (0–160 ng) in the presence of radiolabeled suc-CoA. The radioactivity incorporated was quantified by liquid scintillation counting. The plot displays average counts per minute (CPMs), ± SD and individual datapoints of two independent replicates. Note that increasing enzyme concentrations resulted in increased succinylation.

D, E   *In vitro* desuccinylation assay on H3K122succ peptides with recombinant SIRT7 (D) and SIRT5 (E). Unmodified H3K122 peptide was used as control (left dot). Peptides were probed with H3K122succ AB #2 after incubation with sirtuins. For additional controls, see Fig EV3F and G.

F   H3K122succ levels in *Sirt5*-KO cells. Histones were acid extracted from wild type (WT) and *Sirt5*-KO MEFs, and the levels of H3K122succ determined by immunoblot. The level of H3K122succ was normalized to histones extracted from WT MEFs. Average, ± SD, and individual datapoints of three biological replicates are shown. *P*-value was calculated by two-tailed paired *t*-test.

from WT and *Sirt*5-KO mouse embryonic fibroblasts (MEFs (Park *et al*, 2013); Fig 3F). In accordance with our *in vitro* desuccinylase assay, the levels of H3K122succ were higher in the *Sirt*5-KO MEF cell line compared to the WT, identifying SIRT5 as a novel enzyme that can desuccinylate H3K122 both *in vitro* and *in vivo*.

H3K122succ stimulates transcription *in vitro*

The location of H3K122 at the dyad axis prompted us to investigate the effect of H3K122succ on transcription in a well-controlled system. For this purpose, we performed *in vitro* transcription (IVT) assays (Orphanides *et al*, 1998) on unmodified chromatin templates or chromatin site-specifically succinylated on H3K122. Briefly, we expressed WT H2A, H2B, and H4 in *E. coli* and purified the histones. Site-specifically modified H3K122succ, as well as unmodified H3, were generated by protein synthesis. We assembled chromatin on a pG5-MLP plasmid (Dignam *et al*, 1983), with the help of the nucleosome assembly protein (NAP1) histone chaperone and the ATP-dependent chromatin assembly factor (ACF) remodeling complex (Ito *et al*, 1997). To control for chromatin assembly efficiency, we performed MNase digestion and sucrose gradient fractionation on the assembled chromatin (Fig EV4A and B). The scheme of the general *in vitro* transcription reaction is shown in Fig 4A.

First, we investigated whether adding suc-CoA to the reaction can stimulate transcription and how its effect compares to adding ac-CoA, which is required for efficient transcription on chromatinized templates. For this, we performed *in vitro* transcription on unmodified chromatin in the presence of ac-CoA or suc-CoA or with no CoA. Our results show that not only ac-coA but also suc-CoA can stimulate transcription (Fig 4B and C). Next, in order to study the impact of site-specific H3K122succ on transcription, we performed *in vitro* transcription on unmodified and H3K122succ chromatin. Remarkably, we observed in our assays that the presence of H3K122succ stimulated transcription (compared to unmodified chromatin) by approximately 1.6-fold (Fig 4D and E). Together, these results add H3K122succ to the so far very few examples of site-specific histone modifications whose presence is sufficient to stimulate transcription.

It has been previously shown that most individual acetylations of the H3 tail residues do not affect transcription *in vitro*; however, the acetylation on the lateral surface of the histone octamer at H3K122 can stimulate transcription by approximately 1.7-fold (Tropberger *et al*, 2013). Thus, the two H3K122 modifications—acetylation and succinylation—stimulate transcription *in vitro* to a similar extent.

Succinylation of H3K122 decreases nucleosome stability

We hypothesized that the stimulation of transcription by H3K122-succ could be due to a weakening of DNA histone interactions and, thus, destabilization of nucleosomes. To investigate such a mechanism, we explored the effects of H3K122succ on nucleosome stability by single molecule Förster resonance energy transfer (smFRET) assays. We inserted FRET labels in the nucleosomal DNA (at positions F-48 and R-28, Fig EV5A), assembled mononucleosomes with synthesized H3, either unmodified (Fig 5A top panel) or H3K122succ (Fig 5A bottom panel), and performed

smFRET measurements under different NaCl concentrations. The merged smFRET efficiency histograms (Fig 5A) showed a peak at a FRET efficiency of around $E = 0.8$ representing the intact nucleosomes and a no-FRET peak representing free DNA or a very open nucleosome conformation. As expected, increased salt concentrations led to a reduction of the nucleosome peak. Interestingly, at intermediate salt concentrations the nucleosome population is reduced for H3K122succ-containing nucleosomes compared to unmodified H3-containing nucleosomes. Calculating the normalized fraction of FRET events in the nucleosome population ($E \geq 0.45$; Fig 5B) revealed that H3K122succ nucleosomes are indeed more sensitive to destabilization by increased NaCl concentrations. Determining the NaCl concentration at which half of the nucleosomes have opened (x_0) showed a Δx_0 of -0.12 M NaCl for H3K122succ compared to unmodified nucleosomes (see Materials and Methods for details). Together, these results reveal that H3K122succ nucleosomes are less stable than unmodified nucleosomes, possibly rendering the underlying DNA more accessible and, therefore, facilitating transcription. This is in line with reports of SIRT7-mediated chromatin condensation in cells upon DNA damage (Li *et al*, 2016).

We next wanted to investigate the effects of H3K122ac on nucleosome stability in a similar setup. We, therefore, performed smFRET assays with nucleosomes containing recombinantly expressed WT H3, H3K122ac, and H3K122E, where the latter was previously used to mimic H3K122succ (Li *et al*, 2016). As expected, we observed a reduced stability of the H3K122ac nucleosomes (Δx_0 of -0.05 M NaCl; Fig EV5B and C). The stability of H3K122E nucleosomes was similar to the corresponding WT H3-containing nucleosomes. Although glutamate inverts the charge of the side chain similarly to lysine succinylation, our results suggest that the shorter amino acid side chain of glutamate (compared to lysine) could prevent the H3K122E mutant from being an effective mimic of a succinylated lysine in nucleosome stability assays. Indeed, this is in line with previously reported H3 lysine acetylation mimics that did not fully recapitulate the effects of acetylation (Suganuma & Workman, 2008). When comparing our results between H3K122ac and H3K122succ nucleosomes, it is notable that although H3K122succ nucleosomes are destabilized more than H3K122ac nucleosomes (Fig EV5D and E), the increased instability, compared to H3K122ac, does not translate into increased transcriptional output. This suggests that there is a degree of nucleosomal destabilization that provides maximal transcription output and that further destabilization might have no additional effect on transcription, at least *in vitro*, possibly because transcription is an active process with multiple energy barriers, not simply depending on nucleosome opening.

Our results show that succinylation of H3K122 can be mediated by p300/ CBP, leading to nucleosome destabilization and possible displacement of the histone octamer from the DNA, resulting in increased DNA accessibility. This process is particularly important at regulatory regions such as TSS, suggesting that H3K122succ can facilitate the binding of transcriptional factors resulting in transcriptional activation and maintenance of active transcription. Conversely, the desuccinylation of H3K122succ by SIRT5 (or SIRT7 (Li *et al*, 2016)) leads to chromatin stabilization and compaction, decreasing, thereby DNA accessibility (Fig 5C). Thus, we gained for the first-time insights into the role of a site-specific histone
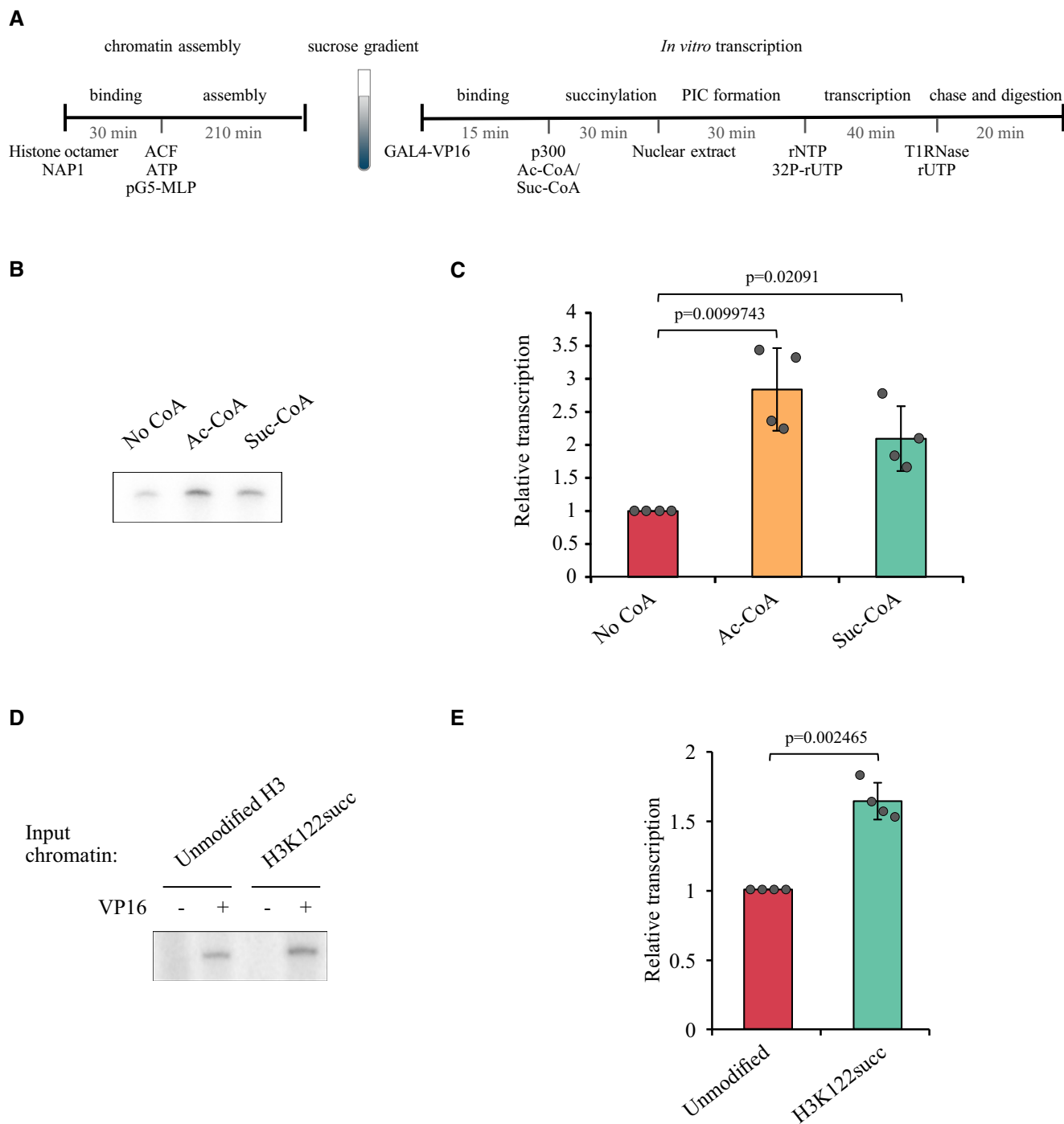
A

chromatin assembly   sucrose gradient   *In vitro* transcription

binding   assembly   binding   succinylation   PIC formation   transcription   chase and digestion

30 min   210 min   15 min   30 min   30 min   40 min   20 min

Histone octamer   ACF   GAL4-VP16   p300   Nuclear extract   rNTP   T1RNase
NAP1   ATP   Ac-CoA/   32P-rUTP   rUTP
pG5-MLP   Suc-CoA

B

C

D

Input chromatin:

E

Figure 4. H3K122suc is sufficient to stimulate transcription.

A   Schematic representation of the IVT assay: chromatin assembly, density selection by sucrose gradient, and *in vitro* transcription per se in the presence of ^{32}P-rUTP. For details, see Materials and Methods.

B   *In vitro* transcription in the presence of GAL4-VP16 and p300, in the presence of no CoA, ac-CoA or suc-CoA. Shown is a representative autoradiogram of the IVT product.

C   Quantification of IVT reactions. Expression relative to no CoA is plotted. Average, ± SD, and individual datapoints of four experiments are shown. *P*-values relative to no CoA were calculated by two-tailed paired *t*-test.

D   *In vitro* transcription on unmodified chromatin or chromatin site-specifically succinylated at H3K122. Shown is a representative autoradiogram.

E   Quantification of IVT reactions. Expression relative to transcription on unmodified chromatin is plotted. Average, ± SD and individual datapoints of four experiments are shown. *P*-value was calculated by two-tailed paired *t*-test.
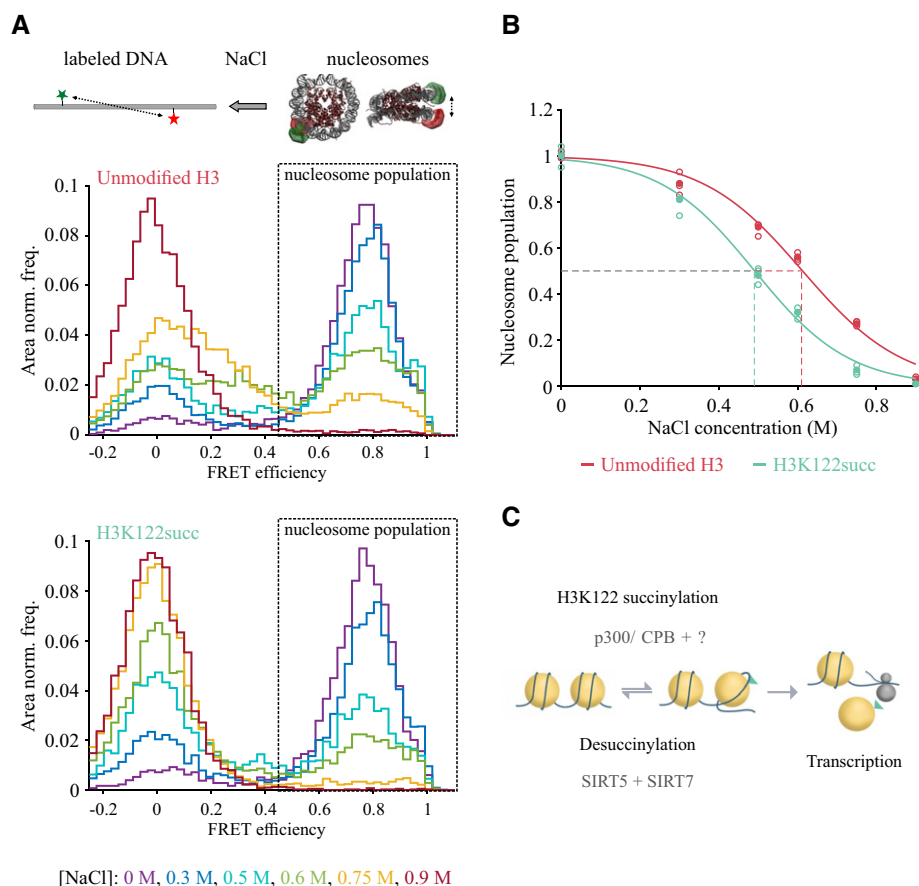
[NaCl]: 0 M, 0.3 M, 0.5 M, 0.6 M, 0.75 M, 0.9 M

Figure 5. H3K122succ can destabilize nucleosomes.

A Schematic representation of the smFRET assay (top), as well as merged smFRET efficiency histograms of unmodified (middle) and H3K122succ mono-nucleosomes (bottom) measured under indicated NaCl conditions (color coded). The nucleosome population is highlighted by the dashed box.

B Fraction of bursts in the nucleosome population (FRET efficiency, $E \geq 0.45$) for unmodified (red, open circles) and H3K122succ nucleosomes (turquoise, open circles) plotted against NaCl concentrations and normalized to the respective mean at 0 M NaCl. Mean values (filled circles) were fitted with the Boltzmann sigmoid function (solid lines) to determine the NaCl concentration where half of the nucleosomes have disassembled (x_0) as 0.61 M (± 0.04) for unmodified and 0.49 M (± 0.03) for H3K122succ nucleosomes.

C Model of H3K122succ function: The establishment of H3K122succ (e.g., by p300/ CBP) favors an open, accessible chromatin state through nucleosome destabilization. Higher DNA accessibility facilitates the binding of the transcriptional machinery and transcription of H3K122succ marked genes. The desuccinylation of H3K122succ, by SIRT5 or SIRT7, results in nucleosome stabilization and reduced transcriptional output.

succinylation in transcription, expanding the role of histone acylations in transcriptional regulation.

We are currently only beginning to understand the links between cellular metabolism and chromatin via histone acylations (Trefely *et al*, 2020). Recently, production of suc-CoA in the nucleus through nuclear oxoglutarate dehydrogenase complex (OGDH) has been reported, allowing α-ketoglutarate conversion to succinyl-CoA, which can be used by the acetyltransferases to succinylate histones (Wang *et al*, 2017). However, it is still unclear whether nuclear, local production of CoAs results in metabolic microniches with increased concentrations of CoAs (Katada *et al*, 2012) that could determine the type of histone acylations to be set on chromatin. Upon changes in CoA availability (e.g. as a consequence of an altered metabolic cell state), specific acylations at the lateral surface of the histone octamer, such as H3K1222succ, at distinct genomic regions, could directly modulate nucleosome stability and thus

transcriptional outcome. Further studies will be required to better understand metabolic regulation of H3K122succ as well as the interplay between different H3K122 acylations.

Materials and Methods

Antibody purification and characterization

For the generation of anti-H3K122succ ABs, rabbits were immunized with the H3K122succ peptide (peptide sequences can be found in Table 1) according to the immunization protocol from BioGenes Gmbh (Germany). Specific ABs were affinity purified from rabbit serum in a two-step purification protocol using SulfoLink™ Coupling Resin (Thermo Fisher Scientific, USA): initially enriching for ABs specific for H3K122succ and later eliminating ABs recognizing H3K122un.

Table 1. List of peptides used in this study.

Peptide abbreviation	Peptide name	Peptide sequence
H3K9ac	H3K9 acetylation	TKQTAR-Kac-STGGKAGC
H3K18ac	H3K18 acetylation	GGKAPR-Kac-QLATKAGC
H3K27ac	H3K27 acetylation	ATKAAR-Kac-SAPATGC
H3K56ac	H3K56 acetylation	IRRYQ-Kac-STELLIGGC
H3K64ac	H3K64 acetylation	STELLIR-Kac-LPFQRLVGC
H3K115ac	H3K115 acetylation	CAIHA-Kac-RVTIMPK
H3K122un	H3K122 unmodified	CGGVTIMP-K-DIQLA
H3K122succ	H3K122 succinylation	CGGVTIMP-Ksuc-DIQLA
H3K122ac	H3K122 acetylation	CGGVTIMP-KAc-DIQLA
H3K122glut	H3K122 glutarylation	CGGVTIMP-Kglut-DIQLAR
H3K122crot	H3K122 crotonylation	CGGVTIMP-Kcrot-DIQLAR

For AB characterization by peptide dot blot, serial dilutions of differently modified peptides (Table 1) were directly spotted onto 0.1 μm-pore nitrocellulose membranes. After completely air-dried, the membranes were blocked with 4% BSA-TBST (0.5% Tween®20) for 1 h at room temperature and probed with ABs, at 1:1,000 dilution, O/N at 4°C. Regarding the characterization by immunoblot, histone acidic extracts were used (Di Cerbo *et al*, 2014). The primary AB was diluted 1:1,000 in 4% BSA-TBST (0.25% Tween®20), and for competition experiments, the diluted AB was pre-incubated on ice with 200 pmol/ml of competitor peptide for 30 min prior to adding to the membrane.

Cell culture

All cells were maintained at 37°C in a humidified atmosphere containing 5% CO_2. MCF7 and HEK293 were grown in low-glucose DMEM, supplemented with 10% fetal bovine serum (FBS), 2 mM L-glutamine, 100 U/ml penicillin, and 0.1 mg/ml streptomycin. MEFs were cultured in high-glucose DMEM, supplemented with 15% FBS, 1× pyruvate, 20 mM HEPES, 100 μM non-essential amino acids, 2 mM L-glutamine, 100 U/ml penicillin, and 0.1 mg/ml streptomycin.

For p300/ CBP inhibition, MCF7 cells were treated with 40 μM curcumin (previously shown to inhibit p300 significantly (Zhang *et al*, 2015)) O/N, followed by histone extraction and quantification of H3K122 succinylation levels by immunoblot. H3K122succ signal was quantified by Image Lab™ and normalized to the corresponding loading control (ponceau staining of membrane).

Native chromatin immunoprecipitation

ChIP on native chromatin was performed as described previously with minor modifications (Daujat *et al*, 2009). For H3K122succ, chromatin immunoprecipitation was performed independently with

three different antibodies from a batch of native chromatin; the H3K9ac, H3K27ac, and H3K4me3 ChIP were performed in one replicate since comparable data have already been reported for MCF7 cells. MCF7 (5×10^7–5×10^8 cells) grown with 10% FBS was collected and washed with PBS. Cell pellets were resuspended in 4 ml of buffer I (0.3 M sucrose; 60 mM KCl 15 mM NaCl; 5 mM $MgCl_2$; 0.1 mM EDTA; 15 mM Tris–HCl, pH 7.5; 0.5 mM DTT; 0.1 mM AEBSF; 5 mM sodium butyrate; 5 mM nicotinamide; 1× cOmplete™ protease inhibitors) and divided into two tubes. Next, 2 ml of buffer II (buffer I supplemented with 0.4% IGEPAL CA-630® (Sigma-Aldrich, USA)) was added to each tube. Samples were gently mixed and incubated on ice for exactly 10 min. The samples were carefully layered on top of 8 ml of sucrose cushion (buffer I with 1.2 M sucrose) and centrifuged in a swing-out rotor at 10,000 *g* for 20 min at 4°C. The supernatant was carefully removed, and the pellets were resuspended in 1 ml of MNase digestion buffer (0.32 M sucrose; 50 mM Tris–HCl, pH 7.5; 4 mM $MgCl_2$; 1 mM $CaCl_2$; 0.1 mM AEBSF). Chromatin was fractionated by MNase digestion (at a final concentration of 2 U/ml) for 7–12 min at 37°C, which is known to release accessible chromatin first. The digestion was stopped with the addition of 5 mM EDTA.

Soluble chromatin fractions were collected by centrifugation of digested chromatin at 12,000 *g* for 10 min. The supernatant (S1) was collected, while the pellet was resuspended in the same volume of dialysis buffer (1 mM Tris–HCl, pH 7.5; 0.2 mM EDTA; 0.2 mM AEBSF; 5 mM sodium butyrate; 5 mM nicotinamide) and dialyzed O/N against dialysis buffer. On the next day, the samples were centrifuged as before and the supernatant was collected (S2). Both fractions underwent quality control on an agarose gel electrophoresis.

Per IP, 40 μg of digested chromatin (20 μg of S1 + 20 μg of S2) was diluted in 500 μl of ChIP incubation buffer (50 mM NaCl; 50 mM Tris–HCl, pH 7.5; 0.1 mM AEBSF; 5 mM EDTA; 5 mM sodium butyrate; 5 mM nicotinamide). The input chromatin was pre-cleared by incubation with 5 μl of dynabeads for 1 h at 4°C. The samples were then incubated O/N at 4°C with different amounts of AB. To each sample, 20 μl of 50% protein A 50% protein G Dynabeads® was added and incubated on a rotating wheel for 2–4 h. The beads were washed 3 times with ChIP incubation buffer, before being eluted with 2 × 125 μl of elution buffer (50 mM NaCl; 50 mM Tris–HCl, pH 7.5; 0.1 mM PMSF; 5 mM EDTA; 1% SDS (w/v)). The samples were then digested with RNase A (Fermentas, USA) for 30–45 min at 37°C and then purified using the QIAquick PCR Purification columns (Qiagen, Germany) according to the manufacturer's instructions.

ChIP-seq library preparation

ChIP samples were purified using Agencourt AMPure XP beads (Beckman Coulter) and quantified with the Qubit (Invitrogen). For the H3K122succ samples and respective input, the ChIP-seq libraries were prepared from 5 to 10 ng of double-stranded purified DNA using the MicroPlex Library Preparation kit v2 (C05010014, Diagenode s.a., Seraing, Belgium), according to manufacturer's instructions. While for H3K4me3, H3K9ac, H3K27ac, and respective input, the ChIP-seq libraries were prepared from 5 ng of double-stranded purified DNA using the NEBNext® Ultra II (E7645S, New England Biolabs). In the first step, the DNA was repaired and yielded molecules with blunt ends. In the next step, stem-loop adaptors with

blocked 5′ ends were ligated to the 5′ end of the genomic DNA, leaving a nick at the 3′ end. The adaptors cannot ligate to each other and do not have single-strand tails, avoiding non-specific background. In the final step, the 3′ ends of the genomic DNA were extended to complete library synthesis and Illumina compatible indexes were added through a PCR amplification (8 cycles). Amplified libraries were purified and size-selected using Agencourt AMPure XP beads (Beckman Coulter) to remove unincorporated primers and other reagents. Libraries were sequenced on Illumina Hiseq 4000 sequencer as single-end 50 bp reads (H3K122succ samples and respective input) or 2 × 100 bp reads (H3K4me3, H3K9ac, H3K27ac, and respective input) following Illumina's instructions. Image analysis and base calling were performed using RTA 2.7.3 and bcl2fastq 2.17.1.14.

ChIP-seq analysis

In this study, the generated ChIP-seq data and published data (see Table 2) were mapped to the human genome (assembly hg38) using Bowtie v1.0.0 (Langmead *et al*, 2009) with default parameters except for "-p 3 -m 1 –strata –best". Peak calling was performed using MACS2 with default parameters for H3K9ac and H3K4me3 except for « -g hs ». For H3K27ac data, MACS2 was run using the following parameters « -g hs --broad --broad-cutoff 0.1 ». Peaks

falling into ENCODE blacklisted regions were removed. Peaks were annotated relative to genomic features using Homer v4.11.1 (Sven *et al*, 2010) (annotations were extracted from gtf file downloaded from Ensembl v94) and using the Bioconductor package ChIPseeker v1.20 (Yu *et al*, 2015). Random distribution of genomic features was obtained by randomly selecting genomic regions of the same amount and width as in the H3K122succ AB #2 peak set with Bedtools shuffle v2.26.0 Quinlan and Hall (2010). Picked regions were covered by at least one read in the input sample to avoid selecting regions in closed chromatin. Heatmaps at genomic loci were generated with seqMINER v1.3.3g (Ye *et al*, 2011). Other heatmaps and boxplots were generated using the R package ggplot2 v3.3 (Wickham, 2016). Venn diagrams were generated using the Bioconductor package DiffBind v2.12 (Ross-Innes *et al*, 2012) with R package VennDiagram v3.6.20.

For the comparison of our ChIP-seq dataset with the H3K122ac, H2A.Z, H2A.Zac, and p300 datasets, as well as for comparing the expression between H3K122succ and H3K122ac marked genes, we used only genes that did not show growth condition dependent changes in their expression (MCF7 grown in 10% FBS versus starved conditions with 5% charcoal-stripped FBS). For this, we used RNA-seq data and read counts per gene normalized across samples using the median-of-ratios method proposed by Anders and Huber (Anders & Huber, 2010) to make the read counts comparable

Table 2. List of publicly available datasets used in this study.

Dataset name	GEO data	Year	Authors	Link
MCF7_RNA-seq	GSM3110713	2019	Handa T, Katayama A, Yokobori T, Yamane A, Fujii T, Obayashi S, Kurozumi S, Kawabata-Iwakawa R, Gombodorj N, Nishiyama M, Asao T, shirabe K, Kuwano H, and Oyama T	https://www.ncbi.nlm.nih.gov/geo/query/acc.cgi?acc=GSM3110713
MCF7_NS_FAIRE_rep1	GSM1825697	2016	Hardy K, Wu F, Tu W, Zafar A, Boulding T, McCuaig R, Sutton C R, Theodoratos A, Rao S	https://www.ncbi.nlm.nih.gov/geo/query/acc.cgi?acc=GSM1825697
MCF7 Dnase-seq	GSM2476264	2017	Liu Y, Chen S, Wang S, Soares F, Fisvher M, Meng F, Du Z, Lin C, Meyer C, DeCaprio J A, Brown M, Liu X S, He H H	https://www.ncbi.nlm.nih.gov/geo/query/acc.cgi?acc=GSM2476264
p300_ChIP	GSM1059392	2013	Tropberger P, Pott S, Keller C, Kamieniarz-Gdula K, Caron M, Richter F, Li G, Mittler G, Liu E T, Bühler M, Margueron R, Schneider R	https://www.ncbi.nlm.nih.gov/geo/query/acc.cgi?acc=GSM1059392
H3K122Ac_ChIP	GSM1059385	2013	Tropberger P, Pott S, Keller C, Kamieniarz-Gdula K, Caron M, Richter F, Li G, Mittler G, Liu E T, Bühler M, Margueron R, Schneider R	https://www.ncbi.nlm.nih.gov/geo/query/acc.cgi?acc=GSM1059385
MCF7_H2A.Z_ChIP	GSM1059387	2013	Tropberger P, Pott S, Keller C, Kamieniarz-Gdula K, Caron M, Richter F, Li G, Mittler G, Liu E T, Bühler M, Margueron R, Schneider R	https://www.ncbi.nlm.nih.gov/geo/query/acc.cgi?acc=GSM1059387
MCF7_H2A.Zac_ChIP	GSM1059388	2013	Tropberger P, Pott S, Keller C, Kamieniarz-Gdula K, Caron M, Richter F, Li G, Mittler G, Liu E T, Bühler M, Margueron R, Schneider R	https://www.ncbi.nlm.nih.gov/geo/query/acc.cgi?acc=GSM1059388

between samples. The comparison between the conditions was performed with the Bioconductor package DESeq2 v1.6.3 with R v3.1.1. Genes having a |log2FC| ≥ 1 and a *P*-value < 0.05 were considered as differentially expressed and thus excluded from further analysis.

Expressed genes (at least one read in RNA-seq) with H3K122succ and H3K122ac peaks (± 500 bp from their TSS) were compared based on their Ensembl Gene IDs, and results are shown as a Venn diagram created by using R scripts.

CGI positions were extracted as a BED file using table cpgIslandExt of the UCSC table browser. CGIs were annotated relative to Ensembl v94 genomic features using Homer v4.11.1 (Sven *et al*, 2010). Genes having H3K122succ peaks and CGIs at their TSS regions were compared based on their Ensembl Gene IDs, and results are shown as a Venn diagram created using R scripts.

Gene symbols of genes associated to H3K122succ peaks were compared to the human housekeeping gene list from: https://www.tau.ac.il/~elieis/HKG/HK_genes.txt (Eisenberg & Levanon, 2013).

RNA-seq analysis

Reads were mapped onto the hg38 assembly of *Homo sapiens* genome using STAR version 2.5.3a (Dobin *et al*, 2013). Gene expression quantification was performed from uniquely aligned reads using htseqcount version 0.6.1p1 (Anders *et al*, 2015), with annotations from Ensembl v94 and "union" mode. Read counts have been normalized across samples with the median-of-ratios method proposed by Anders and Huber (Anders & Huber, 2010), to make these counts comparable between samples.

siRNA KD

Depletion of HAT enzymes was achieved by transient transfection using Lipofectamine™ RNAiMAX (Thermo Fisher Scientific, USA) combined with a reverse transfection protocol following the supplier's instructions. The following ON-TARGETplus SMARTpools from Dharmacon (Horizon Discovery, UK) were used: p300, L-003486-00-0010; CBP, L-003477- 00-0010; pCAF, L-005055-00; GCN5, L-009722-00; scramble negative control, D-001810-10. In brief, a mixture of 10–50 nM of siRNA and lipofectamine was pre-incubated for 20 min at room temperature and mixed with MCF7 cells before plating them. Cells were grown for 72 h.

p300 purification

His-tagged p300 was expressed on baculovirus-infected Sf9 insect cells. After expression, the cells were harvested by centrifugation for 5 min at 400 *g* at 4°C. Unless stated otherwise, all steps were carried out on ice. The cell pellet was resuspended in 2.5 ml of buffer B (20 mM Tris–HCl, pH 7.5; 250 mM NaCl; 0.1% IGEPAL CA-630; 30 mM imidazole; 1× cOmplete™ EDTA-free protease inhibitor cocktail) and dounce homogenized with 10 strokes using an "A" pestle. The sample was incubated on ice for 15 min before being aliquoted into 700–800 μl aliquots and sonicated on a Branson sonicator (3 series of 5 min, with 90% amplitude, 30 s ON and 30 s OFF). The aliquots were pooled together and centrifuged for 15 min at 16,000 *g* at 4°C. The clarified supernatant was loaded on a pre-equilibrated 1 ml HisTrap™ HP column (GE

Healthcare, USA) connected to an Äkta™ pure. After loading, the column was washed with buffer B and eluted with 10 column volumes (CV) of elution buffer (20 mM Tris–HCl, pH 7.5; 100 mM NaCl; 0.1% IGEPAL CA-630; 250 mM imidazole; 10% glycerol; 1× cOmplete™ EDTA-free protease inhibitor cocktail). 500 μl fractions were collected during the elution. The different fractions were analyzed on a 4–12% SDS–PAGE gel followed by coomassie staining. The fractions containing the purified p300 were pooled together and diluted with 50% glycerol before being aliquoted and snap-frozen in liquid nitrogen. The aliquots were stored at −80°C.

Succinyltransferase assays

For the *in vitro* succinyltransferase assays on octamers, 1 μg of recombinant octamers was incubated with 40 ng of p300 in the presence of suc-CoA O/N at 30°C. The reaction products were separated by SDS–PAGE and analyzed by immunoblotting with anti-H3K122succ AB #2. For the succinyltransferase assays on H3K122 peptides, the samples were incubated with 0–160 ng of p300 in the presence of approximately 17 μCi/ml of radiolabeled suc-CoA (American Radiolabeled Chemicals, USA) O/N at 30°C. The reactions were spotted on cellulose chromatography paper P81. Chromatography papers were washed three times with 10% TFA before the incorporated radioactivity was measured by liquid scintillation counting. For "competition assays" on WT H3, 0.5 μg of H3 was incubated with 40 ng of p300 in the presence of approximately 17 μCi/ml of [3H]ac-CoA (Hartmann Analytic, Germany). Unlabeled ac-CoA or suc-CoA (0-70.4 mmol) was added as "competitor" to the reaction. After 4 h of incubation, the reactions were stopped, and the samples ran on an 18.7% SDS–PAGE gel and transferred to a 0.45 μm nitrocellulose membrane. The membrane was air-dried before being exposed to a detection screen. The results were read on an Amersham™ Typhoon™ Biomolecular Imager and signal intensities quantified. In all of these assays, the final reaction buffer consisted of 5% glycerol; 50 mM Tris, pH 8; 0.1 mM EDTA; 7.5 mM sodium butyrate; 7.5 mM nicotinamide; 1 mM DTT; and 1× cOmplete™ protease inhibitors (Roche, Switzerland).

Desuccinylation assays

For the *in vitro* desuccinylation assays, 1 μg of H3K122succ peptides was incubated with 0.5–1.8 μg of SIRT5 or SIRT7 in reaction buffer (20 mM Tris–HCl, pH 7.5; 1 mM DTT) supplemented, or not, with NAD⁺. After 3 h at 37°C, 2 μl of each reaction was spotted on 0.1 μM-pore nitrocellulose membrane and probed with AB anti-H2K122succ #2.

NAP1 purification

NAP1 was purified from cell pellets of baculovirus-infected Sf9 insect cells expressing N-terminally His-tagged NAP1 as previously described (Peterson, 2009). Briefly, after harvesting the cells by centrifugation, the cell pellet was washed with ice-cold PBS. All subsequent steps were performed on ice unless stated otherwise. The cell pellet was resuspended in lysis buffer (50 mM sodium phosphate, pH 7.6; 500 mM NaCl; 20 mM imidazole; 15% glycerol; 0.01% NP40; 10 mM β-glycerophosphate; 0.2 mM PMSF; 0.5 mM

benzamidine-HCl) in 1/40 of the initial cell culture volume and homogenized on a Branson sonicator (3 series of 1 min, with 50% amplitude, 0.5 s ON, and 0.5 s OFF). The sample was cleared by centrifugation for 10 min at 15,000 g at 4°C, and the supernatant was loaded on a pre-equilibrated 5 ml HisTrap™ HP column (GE Healthcare, USA) connected to an Äkta™ pure. After loading the sample, the column was washed with lysis buffer and with wash buffer (50 mM sodium phosphate, pH 7.6; 100 mM NaCl; 20 mM imidazole; 15% glycerol; 0.01% NP40; 10 mM β-glycerophosphate; 0.2 mM PMSF; 0.5 mM benzamidine-HCl). NAP1 was eluted with 42 ml of elution buffer, and fractions of 500 μl were collected and analyzed on an SDS–PAGE gel. The fractions containing NAP1 were pooled together and dialyzed against two changes of 4 l of dialysis buffer (25 mM HEPES, pH 7.6; 1 mM EDTA; 10% glycerol; 100 mM NaCl; 0.01% NP40; 10 mM β-glycerophosphate; 1 mM DTT; 0.2 mM PMSF), where the first dialysis was carried out O/N and the second for 2 h and against one change of 4 l of NAP1 buffer (10 mM HEPES, pH 7.6; 1 mM KCl; 1.5 mM MgCl$_2$; 0.5 mM EDTA; 10% glycerol; 0.01% NP40; 10 mM β-glycerophosphate; 1 mM DTT; 0.2 mM PMSF) plus 100 mM NaCl for 2 h.

After dialysis, any precipitate was removed by centrifugation for 20 min at 20,000 g. The soluble protein was quantified on an 8% SDS–PAGE gel followed by coomassie staining, using BSA as a mass standard. The sample was loaded on a pre-equilibrated 6 ml Resource™ Q (GE Healthcare, USA) column connected to an Äkta™ pure. The column was washed with NAP1 buffer plus 200 mM NaCl and eluted with a 20 CV of a linear gradient from NAP1 buffer supplemented with 200 mM NaCl to NAP1 buffer plus 500 mM NaCl. Fractions of 0.5 ml were collected during elution and analyzed on an 18% SDS–PAGE gel. The fractions corresponding to the first peak contained a 14 kDa contaminant in addition to the 65 kDa NAP1 band. The 14 kDa contaminant corresponds to a NAP1 inhibitor; therefore, all fractions containing any traces of this contaminant were discarded. The fraction corresponding to the second peak, which are contaminant-free, was pooled together and dialyzed against two changes of 2 l of NAP1 buffer plus 100 mM NaCl, for 2 h each. The protein concentration was quantified by SDS–PAGE gel followed by coomassie staining, frozen in liquid nitrogen, and stored at −80°C.

ACF purification

ACF was purified from cell pellets of baculovirus-infected Sf9 insect cells as described (Peterson, 2009). Pellet was resuspended in 8 ml of lysis buffer F (20 mM Tris–HCl, pH 7.9; 500 mM NaCl; 4 mM MgCl$_2$; 0.4 mM EDTA; 2 mM DTT; 20 mM β-glycerophosphate; 20% glycerol; 0.4 mM PMSF; 1 mM benzamidine-HCl; 4 μg/ml leupeptin; 2 μg/ml aprotinin) and dounce homogenized using an "A" pestle (three series of ten strokes over 30 min, on ice). Homogenate was centrifuged for 10 min at 14,500 g at 4°C. The supernatant was transferred to a new tube and mixed with 250 μl of FLAG-M2 resin and 7 ml of dilution buffer F (20 mM Tris–HCl, pH 7.9; 150 mM NaCl; 2 mM MgCl$_2$; 0.2 mM EDTA; 1 mM DTT; 10 mM β-glycerophosphate; 15% glycerol; 0.01% NP40; 0.2 mM PMSF; 0.5 mM benzamidine-HCl; 2 μg/ml leupeptin; 1 μg/ml aprotinin). The slurry mix was incubated for 2–4 h at 4°C on a rotation wheel. After incubation, the samples was centrifuged for 3 min at 775 g at 4°C. The supernatant was removed and the pellet resuspended in 12 ml of wash

buffer F (20 mM Tris–HCl, pH 7.9; 150 mM NaCl; 2 mM MgCl$_2$; 0.2 mM EDTA; 1 mM DTT; 10 mM β-glycerophosphate; 15% glycerol; 0.01% NP40; 0.2 mM PMSF; 0.5 mM benzamidine-HCl; 2 μg/ml leupeptin; 1 μg/ml aprotinin) by tube inversion. The wash was repeated three additional times. For elution, the pellet was resuspended in 100 μl of wash buffer F supplemented with FLAG peptide and insulin (final concentration of 0.4 mg/ml each). The sample was incubated for 10 min on ice and, then, centrifuged for the 30 s at maximum speed. The supernatant containing the purified ACF complex was transferred to a new tube, and elution was repeated two more times. The supernatants were pooled together and aliquoted. Aliquots were frozen in liquid nitrogen and stored at −80°C.

Histone purification and histone octamer assembly

Wild-type recombinant H3, H2A, H2B, and H4, as well as H3K122E and K122R mutants, were expressed in *E. coli* and purified from inclusion bodies (Luger *et al*, 1999). Acetylated H3 at K122 was expressed on *E. coli* through an amber suppression system as previously described (Neumann *et al*, 2009; Tropberger *et al*, 2013). Unmodified H3 and H3K122succ histones were synthesized by Almac (Almac Group, UK). Histone octamers were refolded as described (Luger *et al*, 1999).

In vitro transcription assays

NAP1 and ACF were expressed on baculovirus-infected Sf9 cells and purified as described (Ito *et al*, 1999). Unmodified and H3K122succ chromatin arrays were assembled on pG5-MLP 5S by NAP1 and ACF (Fyodorov & Kadonaga, 2003). Assembled chromatin was purified on a 5–40% sucrose gradient. For *in vitro* transcription assays, per reaction, 50 ng of purified chromatin in 7 μl was mixed with 6 μl of BC100 buffer (20 mM Tris–HCl, pH 7.9; 100 mM KCl; 0.2 mM EDTA; 2% glycerol) and pre-incubated with 50 ng of recombinant GAL4-VP16 for 15 min at room temperature. Next, 40 ng of recombinant p300, as well as 1 μl of a co-enzyme mix (500 nM ac-CoA or suc-CoA/ 200 mM sodium butyrate), was added and incubated for 30 min at 30°C. 10 μl of Hela nuclear extract (prepared as described by Dignam *et al*, 1983) was added, and the reaction was incubated for 30 min at 30°C. A 3 μl mix of ribonucleotides (16.5 μl of 12 mM rATP, rGTP, and rCTP, 5.5 μl rUTP-32P (Perkin BLU007H; Perkin-Elmer, USA), 4.4 μl RNAsin (Promega, USA), and 6.6 μl ddH$_2$O) were added, and transcription was allowed for 40 min at 30°C. The reaction was chased with the addition of a 6 μl rUTP-mix (600 μM cold rUTP and 6 U/μl RNase T1) and incubated for 20 more minutes. The transcribed RNA was phenol-chloroform extracted, precipitated with ethanol, and analyzed on 6% acrylamide denaturing gels (Margueron *et al*, 2008). A phosphor screen was used to capture the signal O/N and was then measured on an Amersham™ Typhoon 5 Biomolecular Imager (GE Healthcare, USA). The signal quantifications were done by ImageJ (Java).

Preparation of double labeled nucleosomes and smFRET assay

Into the 147 bp DNA sequence, based on the MMTV-A sequence, dye molecules were incorporated via PCR with labeled primers (IBA, Table 3). The double labeled DNA was then purified by ethanol precipitation and size exclusion chromatography with a

Table 3. MMTV-A sequence and primer sequences used in the stability assays.

147 bp DNA sequence based on the MMTV-A sequence and primers	Comments
5'- ACTTG CAACA GTCCT AACAT TCACC **T**CTTG TGTGT TTGTG TCTGT TCGCC ATCCC GTCTC CGCTC GTCAC TTA**T**C CTTCA CTTTC CAGAG GGTCC CCCCG C**A**GAC CCCGG CGACC CTCAG GTCGG CCGAC TGCGG CACAG TTTTT TG -3'	**T** Position 0 (dyad) **T** Donor Cy3B attached to T on forward strand (F-48) **A** Acceptor Alexa647 attached to T on reverse strand (R-28)
5'- ACT TGC AAC AGT CCT AAC ATT CAC C**T**C TTG T -3'	**T** Cy3B attached via C6 linker
5'- CAA AAA ACT GTG CCG CAG TCG CCG AC CTG AGG GTC GCC GGG GTC **T**GC GGG -3'	**T** Alexa647 attached via C2 linker

Superose™ 6 Increase 3.2/300 column (GE Healthcare USA). Assembly of double labeled nucleosomes was performed as described earlier (Schwarz *et al*, 2018). In brief, a DNA mixture of the 147 bp labeled DNA (1/10) and unlabeled 200 bp 601 DNA (9/10) in a total concentration of 400 nM was used for the assembly. The unlabeled DNA was used in order to increase the overall nucleosome concentration during single molecule experiments. Additionally, an equal amount of low affinity competitor DNA was used for buffering nucleosome assembly. Purified octamer solution, with specific modifications or unmodified, was titrated against the DNA solution in order to maximize assembly. The nucleosomes were assembled via an O/N salt-gradient dialysis in a TE buffer with DTT (0.25 mM) from the DNA mixture and the histone octamers. For this the Slide-A-Lyzer™ MINI Dialysis Device (7 kDa cutoff, Thermo Fisher Scientific) with the sample was placed in 300 ml of buffer with 2 M NaCl and the salt concentration was reduced stepwise by adding buffer with 50 mM NaCl until about 3 l. Then, a final dialysis step was performed in buffer with 50 mM NaCl. The assembled nucleosomes were analyzed on a 0.4× TBE, 6% PAA gel.

For performing the smFRET measurements, the nucleosomes were diluted to picomolar concentrations of the labeled nucleosomes in measurement buffer containing 10 mM Tris–HCl pH 7.8, 1 mM EDTA, and 0.1 mg/ml BSA with varying NaCl concentrations. The sample was incubated in the buffer for 1.5–2 h on ice, and then, 30 μl was pipetted on a PEG-coated coverslip with restricting the area of the drop by ROTI®Liquid Barrier Marker (Carl Roth, Germany). Salt-dependent nucleosome stability measurements were performed as described before (Bönisch *et al*, 2012). The measurement was performed for 1 h at room temperature on a custom-built confocal microscope which was previously described in detail (Schwarz *et al*, 2018). It uses pulsed interleaved excitation (PIE) in combination with multiparameter fluorescence detection (MFD) (Kudryavtsev *et al*, 2012). The dyes were excited with a green laser (532 nm) and a red laser (640 nm) with an excitation power of 90 μW for both lasers measured before the objective. For each laser, a repetition rate of 20 MHz was used.

The data were analyzed with the software PAM (PIE analysis with MATLAB v1.2) (Schrimpf *et al*, 2018). A burst search (Nir *et al*, 2006) was performed with a minimum threshold of 50 photons per burst, and additionally, at least 5 photons had to be in a time window of 500 μs. To filter for the FRET population, a stoichiometry (raw) cut (0.2–0.85) and an ALEX-2CDE filter (max. 11) (Tomov *et al*, 2012) were applied to those data. After correcting the data for background (between about 0.2 and 0.5 kHz), crosstalk (0.10), direct excitation (0.06), the detection correction factor (0.39), and the excitation correction factor (2.07), a FRET efficiency cut (−0.25 to 1.1) was applied. Due to the design of the dye molecule attachment sites, intact nucleosomes show a peak at a high FRET efficiency and unwrapped nucleosomes show a peak at a FRET efficiency of (close to) zero. The fraction of intact nucleosomes was calculated by dividing the number of events in the nucleosome population (FRET population with a FRET efficiency equal or higher than 0.45) by the overall events in the FRET population. Those values were normalized to the mean value at 0 M NaCl of the respective construct in order to account for a small fraction of free DNA present after assembly.

At least three measurements per sample and salt concentration were performed. After taking the mean, the Boltzmann sigmoid function was fitted to the data $(x) = \frac{1}{1+\exp\left(\frac{x-x_0}{dx}\right)}$, where x_0 is the NaCl concentration where 50% of the nucleosomes have disassembled and dx is a parameter describing the slope of the decay.

Data availability

The ChIP-seq data generated for this study were deposited in the Gene Expression Omnibus (GEO) with accession number GSE152019 (https://www.ncbi.nlm.nih.gov/geo/query/acc.cgi?acc = GSE152019).

Expanded View for this article is available online.

Author contributions

LZS, MH, and SN performed and designed experiments. SLG analyzed the ChIP-seq data. LZS, JM, SD, and RS conceived and designed the project. AM and AG expressed p300, ACF, and NAP1. LZS and RM setup and performed the IVT experiments. LZS, JM, SLG, SD, and RS wrote the manuscript with input from the other authors.

Conflict of interest

The authors declare that they have no conflict of interest.

References

Anders S, Huber W (2010) Differential expression analysis for sequence count data. *J Biol Chem* 11: 1–12

Anders S, Pyl PT, Huber W (2015) HTSeq-A Python framework to work with high-throughput sequencing data. *Bioinformatics* 31: 166–169

Bao X, Liu Z, Zhang W, Gladysz K, Fung YME, Tian G, Xiong Y, Wong JWH, Yuen KWY, Li XD (2019) Glutarylation of histone H4 Lysine 91 regulates chromatin dynamics. *Mol Cell* 76: 1–16

Bönisch C, Schneider K, Pünzeler S, Wiedemann SM, Bielmeier C, Bocola M, Eberl HC, Kuegel W, Neumann J, Kremmer E *et al* (2012) H2A.Z.2.2 is an alternatively spliced histone H2A.Z variant that causes severe nucleosome destabilization. *Nucleic Acids Res* 40: 5951–5964

Cutter A, Hayes JJ (2016) A brief review of nucleosome structure. *FEBS Lett* 589: 2914–2922

Daujat S, Weiss T, Mohn F, Lange UC, Ziegler-Birling C, Zeissler U, Lappe M, Schübeler D, Torres-Padilla ME, Schneider R (2009) H3K64 trimethylation marks heterochromatin and is dynamically remodeled during developmental reprogramming. *Nat Struct Mol Biol* 16: 777–781

Di Cerbo V, Mohn F, Ryan DP, Montellier E, Kacem S, Tropberger P, Kallis E, Holzner M, Hoerner L, Feldmann A *et al* (2014) Acetylation of histone H3 at lysine 64 regulates nucleosome dynamics and facilitates transcription. *Elife* 3: 1–23

Dignam JD, Martin PL, Shastry BS, Roeder RG (1983) Eukaryotic gene transcription with purified components. *Methods Enzymol* 101: 582–598

Dobin A, Davis CA, Schlesinger F, Drenkow J, Zaleski C, Jha S, Batut P, Chaisson M, Gingeras TR (2013) STAR: ultrafast universal RNA-seq aligner. *Bioinformatics* 29: 15–21

Du J, Zhou Y, Su X, Yu JJ, Khan S, Jiang H, Kim J, Woo J, Kim JH, Choi BH *et al* (2011) Sirt5 is a NAD-dependent protein lysine demalonylase and desuccinylase. *Science* 334: 806–809

Eisenberg E, Levanon EY (2013) Human housekeeping genes, revisited. *Trends Genet* 29: 569–574

Frouws TD, Duda SC, Richmond TJ (2016) X-ray structure of the MMTV-A nucleosome core. *Proc Natl Acad Sci USA* 113: 1214–1219

Fyodorov DV, Kadonaga JT (2003) Chromatin assembly in vitro with purified recombinant ACF and NAP-1. *Methods Enzymol* 371: 499–515

Giaimo BD, Ferrante F, Herchenröther A, Hake SB (2019) The histone variant H2A.Z in gene regulation. *Epigenet Chromatin* 12: 1–22

Hirschey MD, Zhao Y (2015) Metabolic regulation by lysine malonylation, succinylation, and glutarylation. *Mol Cell Proteomics* 14: 2308–2315

Hu A, Britton LM, Garcia BA (2014) Investigating the specificity of histone acetyltransferase activity for producing rare modifications on histones using mass spectrometry. In *Proceedings of the 62nd Annual American Society for Mass Spectrometry Conference on Mass Spectrometry and Allied Topics*, Baltimore

Ito T, Bulger M, Pazin MJ, Kobayashi R, Kadonaga JT (1997) ACF, an ISWI-containing and ATP-utilizing chromatin assembly and remodeling factor. *Cell* 90: 145–155

Ito T, Levenstein ME, Fyodorov DV, Kutach AK, Kobayashi R, Kadonaga JT (1999) ACF consists of two subunits, Acf1 and ISWI, that function cooperatively in the ATP-dependent catalysis of chromatin assembly. *Genes Dev* 13: 1529–1539

Jenuwein T, Allis CD (2001) Translating the histone code. *Science* 293: 1074–1080

Katada S, Imhof A, Sassone-Corsi P (2012) Connecting threads: epigenetics and metabolism. *Cell* 148: 24–28

Kebede AF, Schneider R, Daujat S (2015) Novel types and sites of histone modifications emerge as players in the transcriptional regulation contest. *FEBS J* 282: 1658–1674

Kouzarides T (2007) Chromatin modifications and their function. *Cell* 128: 693–705

Kudryavtsev V, Sikor M, Kalinin S, Mokranjac D, Seidel CA, Lamb DC (2012) Combining MFD and PIE for accurate single-pair förster resonance energy transfer measurements. *ChemPhysChem* 13: 1060–1078

Langmead B, Trapnell C, Pop M, Salzberg SL (2009) Ultrafast and memory-efficient alignment of short DNA sequences to the human genome. *Genome Biol* 10: R25

Lawrence M, Daujat S, Schneider R (2016) Lateral thinking: how histone modifications regulate gene expression. *Trends Genet* 32: 42–56

Li L, Shi LL, Yang S, Yan R, Zhang D, Yang J, He L, Li W, Yi X, Sun L *et al* (2016) SIRT7 is a histone desuccinylase that functionally links to chromatin compaction and genome stability. *Nat Commun* 7: 1–17

Luger K, Mäder AW, Richmond RK, Sargent DF, Richmond TJ, Luger K, Ma AW (1997) Crystal structure of the nucleosome core particle at 2.8 A resolution. *Nature* 389: 251–260

Luger K, Rechsteiner TJ, Richmond TJ (1999) *Expression and purification of recombinant histones and nucleosome reconstitution*, Totowa, NJ: Humana Press

Margueron R, Li G, Sarma K, Blais A, Zavadil J, Woodcock CL, Dynlacht BD, Reinberg D (2008) Ehz1 and Ezh2 maintain repressive chromatin through different mechanisms. *Mol Cell* 32: 503–518

Maurer B, Rumpf T, Scharfe M, Stolfa DA, Schmitt ML, He W, Verdin E, Sippl W, Jung M (2012) Inhibitors of the NAD+-dependent protein desuccinylase and demalonylase sirt5. *ACS Med Chem Lett* 3: 1050–1053

Mersfelder EL, Parthun MR (2006) The tale beyond the tail: histone core domain modifications and the regulation of chromatin structure. *Nucleic Acids Res* 34: 2653–2662

Morimoto T, Sunagawa Y, Kawamura T, Takaya T, Wada H, Nagasawa A, Komeda M, Fujita M, Shimatsu A, Kita T *et al* (2008) The dietary compound curcumin inhibits p300 histone acetyltransferase activity and prevents heart failure in rats. *J Clin Invest* 118: 868–878

Muschielok A, Andrecka J, Jawhari A, Brückner F, Cramer P, Michaelis J (2008) A nano-positioning system for macromolecular structural analysis. *Nat Methods* 5: 965–971

Neumann H, Hancock SM, Buning R, Routh A, Chapman L, Somers J, Owen-Hughes T, van Noort J, Rhodes D, Chin JW (2009) A method for genetically installing site-specific acetylation in recombinant histones defines the effects of H3K56 acetylation. *Mol Cell* 36: 153–163

Nir E, Michalet X, Hamadani KM, Laurence TA, Neuhauser D, Kovchegov Y, Weiss S (2006) Shot-noise limited single-molecule FRET histograms:

comparison between theory and experiments. *J Phys Chem* 110: 22103–22124

Orphanides G, LeRoy G, Chang CH, Luse DS, Reinberg D (1998) FACT, a factor that facilitates transcript elongation through nucleosomes. *Cell* 92: 105–116

Park J, Chen Y, Tishkoff DX, Peng C, Tan M, Dai L, Xie Z, Zhang Y, Zwaans BMMM, Skinner ME *et al* (2013) SIRT5-mediated lysine desuccinylation impacts diverse metabolic pathways. *Mol Cell* 50: 919–930

Peterson CL (2009) Purification of recombinant *Drosophila* ACF. *Cold Spring Harbor Protoc* 4: 1–4

Quinlan AR, Hall IM (2010) BEDTools: A flexible suite of utilities for comparing genomic features. *Bioinformatics* 26: 841–842

Ross-Innes CS, Stark R, Teschendorff AE, Holmes KA, Ali HR, Dunning MJ, Brown GD, Gojis O, Ellis IO, Green AR *et al* (2012) Differential oestrogen receptor binding is associated with clinical outcome in breast cancer. *Nature* 481: 389–393

Santos-Rosa H, Schneider R, Bannister AJ, Sherriff J, Bernstein BE, Emre NCT, Schreiber SL, Mellor J, Kouzarides T (2002) Active genes are tri-methylated at K4 of histone H3. *Nature* 419: 407–411

Schrimpf W, Barth A, Hendrix J, Lamb DC (2018) PAM: a framework for integrated analysis of imaging, single-molecule, and ensemble fluorescence data. *Biophys J* 114: 1518–1528

Schwarz MSK, Kallis E, Eustermann S, Guariento M, Moldt M, Hopfner K-P, Michaelis J (2018) Single-molecule nucleosome remodelling by INO80 and effects of histone tails. *FEBS Lett* 592: 318–331

Suganuma T, Workman JL (2008) Crosstalk among histone modifications. *Cell* 135: 604–607

Sven H, Christopher B, Nathanael S, Eric B, Yin CL, Laslo P, Cheng JX, Murre C, Singh H, Glass CK (2010) Simple combinations of lineage-determining transcription factors prime cis-regulatory elements required for macrophage and B cell identities. *Mol Cell* 38: 576–589

Tan M, Luo H, Lee S, Jin F, Yang JS, Montellier E, Buchou T, Cheng Z, Rousseaux S, Rajagopal N *et al* (2011) Identification of 67 histone marks and histone lysine crotonylation as a new type of histone modification. *Cell* 146: 1016–1028

Tessarz P, Kouzarides T (2014) Histone core modifications regulating nucleosome structure and dynamics. *Nat Rev Mol Cell Biol* 15: 703–708

Tomov TE, Tsukanov R, Masoud R, Liber M, Plavner N, Nir E (2012) Disentangling subpopulations in single-molecule FRET and ALEX experiments with photon distribution analysis. *Biophys J* 102: 1163–1173

Trefely S, Lovell CD, Snyder NW, Wellen KE (2020) Compartmentalised acyl-CoA metabolism and roles in chromatin regulation. *Mol Metab* 38: 1–18

Tropberger P, Pott S, Keller C, Kamieniarz-Gdula K, Caron M, Richter F, Li G, Mittler G, Liu ET, Bühler M *et al* (2013) Regulation of transcription through acetylation of H3K122 on the lateral surface of the histone octamer. *Cell* 152: 859–872

Tropberger P, Schneider R (2013) Scratching the (lateral) surface of chromatin regulation by histone modifications. *Nat Struct Mol Biol* 20: 657–661

Wang Y, Guo YR, Liu K, Yin Z, Liu R, Xia Y, Tan L, Yang P, Lee J-H, Li X-j *et al* (2017) KAT2A coupled with the α-KGDH complex acts as a histone H3 succinyltransferase. *Nature* 552: 273–277

Wickham H (2016) *ggplot2: elegant graphics for data analysis*. New York: Springer-Verlag

Xie Z, Dai J, Dai L, Tan M, Cheng Z, Wu Y, Boeke JD, Zhao Y (2012) Lysine succinylation and lysine malonylation in histones. *Mol Cell Proteomics* 11: 100–107

Ye T, Krebs AR, Choukrallah MA, Keime C, Plewniak F, Davidson I, Tora L (2011) seqMINER: an integrated ChIP-seq data interpretation platform. *Nucleic Acids Res* 39: 1–10

Yu G, Wang LG, He QY (2015) ChIP seeker: an R/Bioconductor package for ChIP peak annotation, comparison and visualization. *Bioinformatics* 31: 2382–2383

Zhang P, Elabd S, Hammer S, Solozobova V, Yan H, Bartel F, Inoue S, Henrich T, Wittbrodt J, Loosli F *et al* (2015) TRIM25 has a dual function in the p53/Mdm2 circuit. *Oncogene* 34: 5729–5738

Zhang ZZ, Tan M, Xie Z, Dai L, Chen Y, Zhao Y, Zhao T, Zhao Y (2011) Identification of lysine succinylation as a new post-translational modification. *Nat Chem Biol* 7: 58–63